Original Article

Virtual unenhanced images derived from dual-energy computed tomography for assessing bone mineral density and detecting osteoporosis

Xiaoyu Tong[1#], Xin Fang[1#], Shigeng Wang[1], Yong Fan[1], Wei Wei[1], Qingzhu Xiao[2], Anliang Chen[1], Yijun Liu[1], Lei Liu[3]

[1]Department of Radiology, First Affiliated Hospital of Dalian Medical University, Dalian, China; [2]School of Investment and Project Management, Dongbei University of Finance and Economics, Dalian, China; [3]Department of Urology, First Affiliated Hospital of Dalian Medical University, Dalian, China

Contributions: (I) Conception and design: X Tong, X Fang; (II) Administrative support: L Liu, Y Liu; (III) Provision of study materials or patients: W Wei, X Tong; (IV) Collection and assembly of data: S Wang, X Fang; (V) Data analysis and interpretation: S Wang, Y Fan, Q Xiao; (VI) Manuscript writing: All authors; (VII) Final approval of manuscript: All authors.

[#]These authors contributed equally to this work.

Correspondence to: Lei Liu, PhD. Department of Urology, First Affiliated Hospital of Dalian Medical University, No. 193 Lianhe Road, Xigang District, Dalian 116011, China. Email: liuleidmu1989@163.com.

Background: The early detection and treatment of osteoporosis can help prevent osteoporosis-related fractures, especially in patients who undergo enhanced computed tomography (CT) scans for disease diagnosis or evaluation of treatment outcomes. Although Hounsfield unit (HU) measurement of the vertebral body has been shown to have a strong positive correlation with bone mineral density (BMD), the contrast media will impact the CT value of the vertebral body and decrease the accuracy. This study is aimed to examine the distinctions in vertebral body CT attenuation measurement on true unenhanced (TUE) and virtual unenhanced (VUE) images generated from triphasic enhanced dual-energy CT (DECT) scans and to determine the feasibility of assessing BMD and detecting osteoporosis on VUE images as compared to quantitative CT (QCT).

Methods: A total of 235 patients underwent abdominal CT examinations that included unenhanced (with 120 kVp and Smart mA) and triphasic enhanced DECT scans. The BMD and CT attenuation values of the L1–L2 vertebrae were measured on TUE and VUE images reconstructed from the triphasic enhanced CT. The differences and associations between TUE and VUE generated from triphasic enhanced CT were analyzed. The diagnostic performances of HU measurements obtained from TUE and VUE images were evaluated using receiver operating characteristic curve.

Results: The BMD and HU measurements of the vertebrae showed good interobserver repeatability on both TUE and VUE images (all intercorrelation coefficients >0.92). The CT attenuation values of L1 and L2 and their average value showed no statistically significant difference among the triphasic VUE images (F=0.121, F=0.061, F=0.090; all P values >0.05) but were significantly lower than those obtained from the TUE images. HU measurements in both the TUE and triphasic VUE images, along with the reference BMD derived from QCT, demonstrated a strong positive correlation (r_{TUE} =0.981, r_{VUEa} =0.966, r_{VUEv} =0.962, r_{VUEd} =0.964; all P values <0.05), with excellent diagnostic performance for the diagnoses of osteoporosis and osteopenia (all areas under curve >0.95). The Bland-Altman scatter plot exhibited good agreement, as the deviations between the reference BMD and the calculated BMD were evenly distributed around 0.

Conclusions: Although the attenuation values of the vertebrae on the VUE images were underestimated compared to those on the TUE images, the HU measurement on VUE image was effective in assessing

BMD and detecting osteoporosis and osteopenia with good diagnostic performance.

Keywords: Bone mineral density (BMD); osteoporosis; Hounsfield units (HU); dual-energy CT (DECT); virtual unenhanced (VUE) images; contrast-enhanced CT

Submitted May 26, 2023. Accepted for publication Aug 09, 2023. Published online Sep 13, 2023.
doi: 10.21037/qims-23-748
View this article at: https://dx.doi.org/10.21037/qims-23-748

Introduction

Osteoporosis is a prevalent chronic metabolic bone disease that is often underdiagnosed (1). It poses a significant health problem for individuals aged over 50 years, particularly older adults and postmenopausal women (2). Unfortunately, most patients only receive a diagnosis once they begin experiencing clinical symptoms such as pain, spinal deformation, and fractures. This delay in diagnosis can hinder the effectiveness of osteoporosis prevention and treatment. With the aging population, the incidence of osteoporotic fractures is expected to rise significantly, from 1.9 million in 2018 to 3.2 million in 2040 (3). This surge in incidence is directly linked to a significant rise in the costs associated with medical treatment and fractures (4). Substantial increase in expenditure places a significant economic burden on individuals and society as a whole.

Dual-energy X-ray absorptiometry (DXA) is the gold standard for the clinical diagnosis of osteoporosis. However, this technique solely measures areal bone mineral density (BMD) which may be erroneously elevated due to factors of degenerative changes such osteophytes and overlapping anatomy (5,6). Compared to DXA, quantitative computed tomography (QCT) possesses more advantages in the early screening of osteoporosis (7). It measures the volumetric BMD of spongy bone, which allows for quantitative analysis and the exclusion of spinal degenerative changes and vascular calcification from BMD assessment (8). QCT is also a reference standard for the accurate diagnosis of osteoporosis. However, due to the requirement of dedicated measurement equipment, additional radiation exposure, and economic costs, QCT is not widely used. There is thus a pressing need to find a safe and cost-effective method for the opportunistic screening of osteoporosis.

Hounsfield unit (HU) measurement of the vertebral body has been shown to have a strong positive correlation with BMD and provides high-quality diagnostic information for clinicians, while involving no additional radiation exposure or economic cost to the patient (9-11). Although HU measurement is not influenced by calcification or osteophyte islands, it is susceptible to scanning parameters and contrast media injection protocols. A retrospective study by Pickhardt *et al.* (12) investigated the effect of iodine contrast media on CT attenuation values of the vertebral body and found that the CT value of the L1 vertebral body increased by 11.2±19.2 HU on enhanced CT compared to unenhanced CT. Therefore, it is not appropriate to use the original diagnostic threshold to distinguish osteoporosis from normal BMD. Additionally, the role of different iodine contrast media intake values has not been taken into consideration. Patients with different diseases, especially those with malignant tumors, often undergo multiple contrast-enhanced scans for disease staging and efficacy evaluation, but no unenhanced images are available for these cases. Individuals with malignant tumors may lose bone faster than many others because of lifestyle or treatment, and opportunistic screening with available imaging data could be beneficial (13,14). Compared with conventional CT, dual-energy CT (DECT) can separate different substances by collecting high- and low-energy information. The material separation algorithm can identify an iodine contrast medium and virtually eliminate its influence to obtain virtual unenhanced (VUE) images (15). Previous studies have demonstrated that VUE images can serve as a potential surrogate for true unenhanced (TUE) images in the identification of certain tissues or lesions (liver, kidney, and fatty liver assessment), reducing the radiation dose administered to patients (16-18). However, for HU measurements in vertebrae, the association and differences between VUE images generated from triphasic enhanced CT and TUE images have not been well established. Therefore, the purpose of this study was dual: first, we investigated the differences between vertebral HU measurements on VUE images generated from triphasic enhanced CT scans and TUE images; second, we aimed to determine the feasibility of assessing BMD and detecting osteoporosis on VUE images via a comparison to QCT.

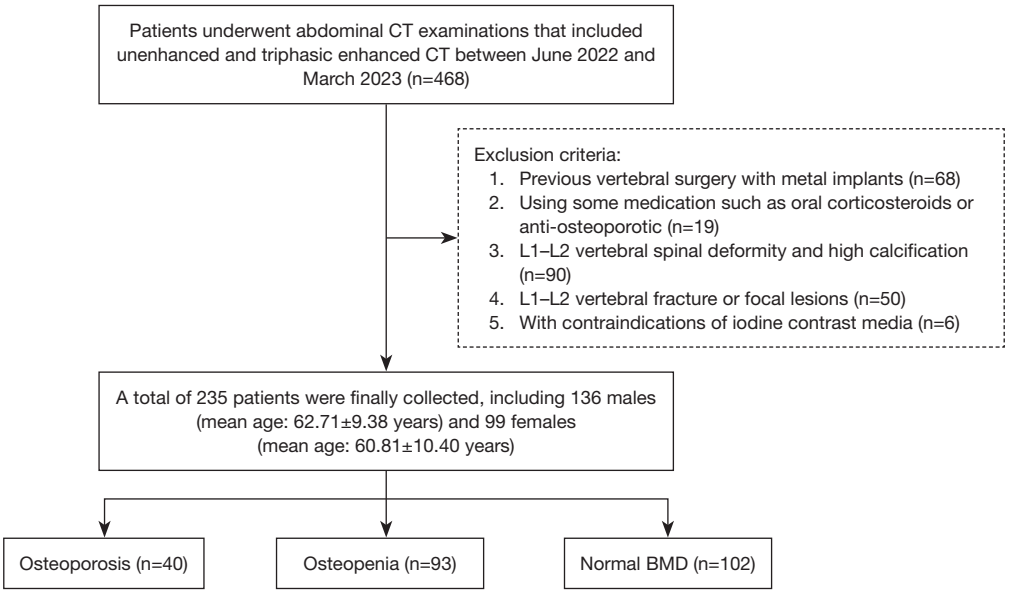

Figure 1 A flowchart of participant enrollment. CT, computed tomography; BMD, bone mineral density.

Methods

Study population

The study was conducted in accordance with the Declaration of Helsinki (as revised in 2013), and the prospective single-center exploratory study design was approved by the Ethics Committee of First Affiliated Hospital of Dalian Medical University (approval No. PJ-KS-KY-2022-43). All patients provided signed informed consent for use of their CT images. A total of 468 consecutive patients who underwent abdominal CT examinations that included TUE and triphasic enhanced CT scans (arterial, portal venous, and delayed phases) between June 2022 and March 2023 were enrolled. Patients with any of the following conditions were excluded: (I) previous vertebral surgery with metal implants (n=68), (II) use of certain medication such as oral corticosteroids or anti-osteoporotic drugs (n=19), (III) with L1–L2 vertebral spinal deformity and high calcification (n=90), (IV) with L1–L2 vertebral fracture or focal lesions (n=50), and (V) contraindications to iodine contrast medium (n=6). *Figure 1* shows a flowchart of the study population.

Images acquisition

All CT scans were performed on a 256-row fast-switching DECT scanner (Revolution CT, GE HealthCare, Chicago, IL, USA). The TUE images were acquired using a fixed tube voltage of 120 kVp and Smart mA (noise index: 10), while triphasic enhanced CT scans were performed using the gemstone spectral imaging (GSI) mode with fast tube voltage switching between 80 and 140 kVp and a tube current of 400 mA. Other scanning parameters were kept constant, including a detector coverage of 80 mm, rotation speed of 0.5 s/r, pitch of 0.992:1, scanning slice thickness and slice interval of 5 mm, and matrix of 512×512. In each patient, the scan length, volumetric CT-dose index ($CTDI_{vol}$) and dose-length product (DLP) were recorded.

For the enhanced CT scans, a nonionic contrast medium (ioversol 320 mgI/mL; Jiangsu Hengrui Pharmaceutical Co., Ltd., Lianyungang, China) was administered via the median cubital vein at a flow rate of 3–4.5 mL/s. The volume of the contrast medium was determined based on the patient's body weight at 500 mgI/kg. Following completion of the contrast injection, 30 mL of saline was injected at the same flow rate. Arterial phase scanning was performed using a threshold of 180 HU in the descending aorta and a delay of 5.9 seconds. Portal venous and delayed phases were acquired 60 and 150 seconds after the arterial phase, respectively. The asynchronous phantom was scanned every week using the same scanning parameters for quality assurance to precisely assess the BMD.

Image reconstruction

The TUE images were reconstructed in the axial plane

with a standard kernel and 40% adaptive statistical iterative reconstruction-Veo (ASIR-V) at a 1.25-mm thickness and interval. Subsequently, the images were transferred to a QCT Pro workstation (QCT pro v. 6.1, Mindways Software, Inc., Austin, TX, USA) and the Advantage Workstation 4.7 dedicated to postprocessing (GE HealthCare) for BMD and HU measurements. The VUE images of arterial (VUEa), portal venous (VUEv), and delayed (VUEd) phases were automatically generated from the CT console. The kernel, the level of ASIR-V, reconstruction thickness, and interval were the same as those used for TUE images.

BMD assessment and HU measurement

To assess the BMD of the L1–L2 vertebrae, an oval volume of interest (VOI) was manually placed on the axial plane using the QCT Pro workstation (Mindways Software, Inc.). The VOI covered approximately two-thirds of the centrum, with a depth of 9 mm. Areas with bone islands, cortical bone, vertebral venous plexus, and osteosclerotic artifacts were excluded from the VOI as much as possible. According to the relevant application guidelines for clinical BMD assessment (19,20), osteoporosis was identified as a BMD below 80 mg/cm^3, osteopenia as a BMD between 80 and 120 mg/cm^3, and normal status as a BMD above 120 mg/cm^3.

HU measurements of the L1–L2 vertebrae were conducted on the triphasic VUE images on the Advantage Workstation 4.7. The region of interest (ROI) was placed on the cancellous bone, carefully avoiding abnormal density artifacts and calcification. The copy-paste function was used to ensure consistent ROI locations for each phase. Statistical analysis was performed by calculating the average BMD and CT attenuation values.

To test the interobserver repeatability, a total of 100 patients were selected randomly, and the BMD and CT attenuation values were measured independently by a junior radiologist with 4 years of diagnostic experience in musculoskeletal radiology and a senior musculoskeletal radiologist with 10 years of diagnostic experience. If the interobserver repeatability was deemed satisfactory, the remaining measurements were carried out by the junior radiologist under the supervision of the senior musculoskeletal radiologist.

Statistical analysis

Data analysis was conducted using SPSS 24.0 (IBM Corp., Armonk, NY, USA) and MedCalc version 20.022 (MedCalc Ltd., Ostend, Belgium). The normality of data was tested using the Kolmogorov-Smirnov test, and continuous data are presented as mean ± standard deviation. The intraclass correlation coefficient (ICC) was used to assess the interobserver agreement for BMD and HU measurements (<0.40, fair; 0.41–0.60, moderate; 0.61–0.80, good; >0.81, excellent). Differences between VUEa, VUEv, and VUEd were compared using 1-way analysis of variance (ANOVA), while differences between TUE and VUE derived from triphasic enhanced CT were assessed using the Student's *t*-test. The Pearson or Spearman correlation test was used to examine the association between the TUE, VUE, and BMD, and the regression equations were established to predict BMD. The agreement between the calculated BMD derived from TUE and triphasic VUE images and the reference BMD was assessed using Bland-Altman plots. Diagnostic accuracy was evaluated using receiver operating characteristic (ROC) curves, and the difference in the area under the curve (AUC) was compared using the DeLong test.

Results

Study population

A total of 235 patients, comprising 136 males (mean age: 62.71±9.38 years) and 99 females (mean age: 60.81±10.40 years), were enrolled in this study. According to the application guidelines (19,20), there were 40 cases of osteoporosis, 93 cases of osteopenia, and 102 cases of normal bone mass, as presented in *Figure 1*. The average scanning length was 427.44±102.84 cm; the $CTDI_{vol}$ and DLP of the conventional 120-kVp unenhanced CT were 9.04±3.34 mGy and 396.79±192.73 mGy·cm, respectively; and the $CTDI_{vol}$ and DLP of arterial, venous, and delayed phases on the GSI mode were 11.98 mGy and 512.07±123.21 mGy·cm, respectively.

Comparison of vertebral body CT values between the TUE and triphasic VUE images

The BMD and HU measurements of the vertebral body showed good interobserver repeatability on both TUE and VUE images (all ICCs >0.92). No statistically significant differences were observed in CT attenuation values measured from the L1–L2 vertebrae and the average CT values among the 3-phase VUE images. However, the CT

attenuation values of the vertebral body measured on the VUE images were significantly lower than those obtained from the TUE images (*Tables 1*,*2*). The HU measurements in both the TUE and triphasic VUE images, along with the reference BMD derived from QCT, showed a strong positive correlation (r_{TUE} =0.981, r_{VUEa} =0.966, r_{VUEv} =0.962, r_{VUEd} =0.964; all P values <0.05), with corresponding adjusted R^2 values of 0.963, 0.932, 0.925, and 0.930 on TUE and triphasic VUE images, respectively. The linear equations are presented in *Figure 2*.

Table 1 Interobserver repeatability on TUE and VUE images

Measurement	Category	ICC	95% CI
L1	BMD	0.940	0.837–0.971
	TUE	0.953	0.931–0.968
	VUEa	0.935	0.905–0.956
	VUEv	0.938	0.909–0.958
	VUEd	0.931	0.899–0.953
L2	BMD	0.942	0.813–0.974
	TUE	0.952	0.928–0.968
	VUEa	0.933	0.901–0.954
	VUEv	0.940	0.912–0.960
	VUEd	0.941	0.914–0.960
Average	BMD	0.945	0.806–0.976
	TUE	0.970	0.955–0.980
	VUEa	0.964	0.948–0.976
	VUEv	0.965	0.949–0.977
	VUEd	0.964	0.948–0.976

TUE, true unenhanced; VUE, virtual unenhanced; ICC, intraclass correlation coefficient; CI, confidence interval; BMD, bone mineral density; VUEa, VUE image from arterial phase; VUEv, VUE image from portal venous phase; VUEd, VUE image from delayed phase.

Diagnostic performance analysis of HU measurements on the VUE images

The CT values of the vertebral body obtained from the TUE and triphasic VUE images were used to diagnose osteoporosis and osteopenia according to the QCT reference standard. The AUC for osteoporosis diagnosis was 0.997 [95% confidence interval (CI): 0.978–1.000] for the TUE images and 0.988 (95% CI: 0.964–0.998), 0.979 (95% CI: 0.952–0.993), and 0.982 (95% CI: 0.956–0.995) for the VUEa, VUEv and VUEd images. The DeLong test demonstrated a statistical difference between the TUE and triphasic VUE images (*Table 3*).

For osteopenia diagnosis, the AUC was 0.989 (95% CI: 0.963–0.999) for the TUE images and 0.971 (95% CI: 0.936–0.990), 0.969 (95% CI: 0.934–0.988), and 0.971 (95% CI: 0.937–0.990) for the VUEa, VUEv and VUEd images. A DeLong test paired comparison revealed a statistical difference in measurement between the TUE and the VUE reconstructed from the venous phase (*Table 4*). The ROC curves are presented in *Figure 3*.

In addition, we conducted a comparative analysis to evaluate the diagnostic accuracy of identifying osteoporosis and osteopenia in TUE and triphasic VUE images. The results from the DeLong test indicated that there was no statistically significant difference (*Table 5*).

The agreement analysis between the reference and calculated BMD

The predicted BMD was calculated using the linear regression equations of TUE and the triphasic VUE images obtained. The Bland-Altman scatter plot showed good agreement, as the deviations between the reference BMD and the predicted

Table 2 Difference of the HU measurement between TUE and triphasic VUE images

Category	TUE	VUEa	VUEv	VUEd	F	P
L1	146.78±51.17	65.81±24.20*	65.49±24.38*	64.73±24.34*	0.121	0.886
L2	140.17±51.36	61.01±24.65*	60.71±24.76*	60.22±24.73*	0.061	0.941
Average	143.47±50.64	63.41±24.05*	63.10±24.19*	62.48±24.20*	0.090	0.913

Data are presented as mean ± standard deviation. *, TUE was compared with triphasic VUE images, P<0.05. HU, Hounsfield unit; TUE, true unenhanced; VUE, virtual unenhanced; VUEa, VUE image from arterial phase; VUEv, VUE image from portal venous phase; VUEd, VUE image from delayed phase.

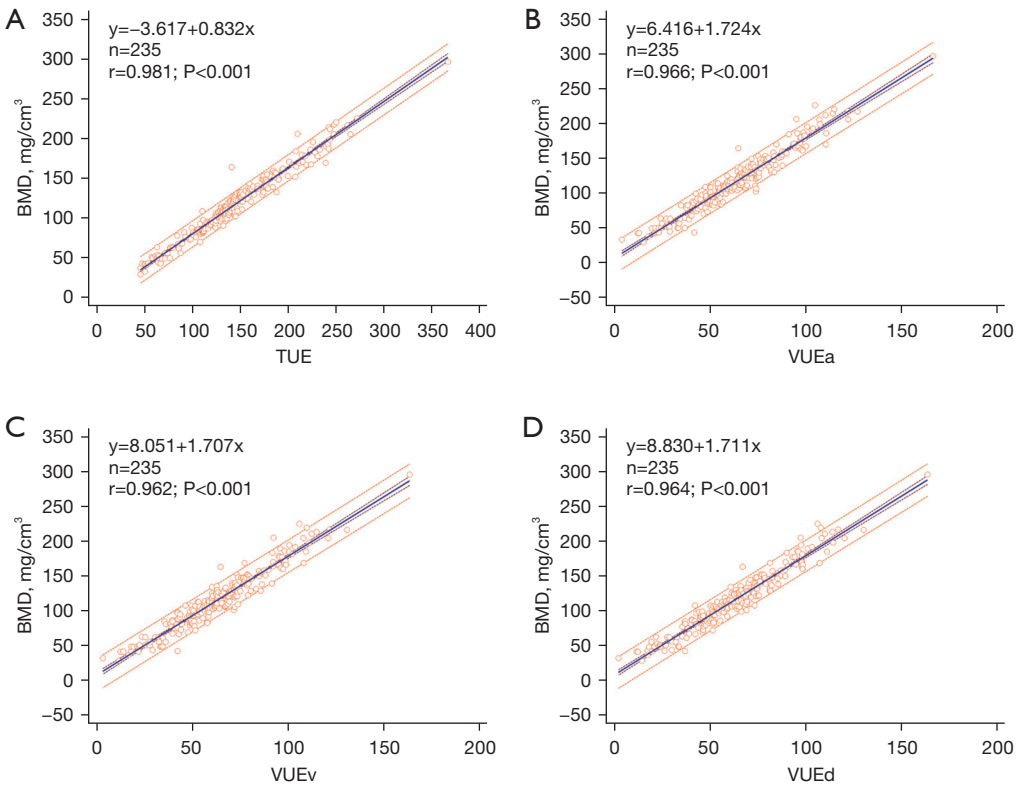

Figure 2 The vertebral body CT attenuation values derived from TUE and VUE images showed a strong association with the reference BMD values, with calibrated R^2 values of 0.963, 0.932, 0.925, and 0.930 on TUE, VUEa, VUEv and VUEd images, respectively. Linear equations were established. The dotted lines in orange show the 95% prediction. CT, computed tomography; BMD, bone mineral density; TUE, true unenhanced; VUE, virtual unenhanced; R^2, adjusted correlation coefficient; VUEa, VUE image from arterial phase; VUEv, VUE image from portal venous phase; VUEd, VUE image from delayed phase.

Table 3 ROC curve analysis of HU measurement for the diagnosis of osteoporosis

Category	Threshold	Sensitivity, %	Specificity, %	AUC	95% CI
TUE	108.65	100.0	95.38	0.997	0.978–1.000
VUEa	47.30	97.5	93.33	0.988	0.964–0.998
VUEv	48.65	95.0	90.26	0.979	0.952–0.993
VUEd	47.50	97.5	89.23	0.982	0.956–0.995

ROC, receiver operating characteristic; HU, Hounsfield unit; TUE, true unenhanced; VUE, virtual unenhanced; VUEa, VUE image from arterial phase; VUEv, VUE image from portal venous phase; VUEd, VUE image from delayed phase; AUC, area under the curve of receiver operating characteristic; CI, confidence interval.

BMD were evenly distributed around 0 (*Figure 4*).

Discussion

In this study, we conducted a comprehensive evaluation of the difference in CT attenuation values of the L1–L2 vertebral cancellous bone between the TUE and VUE images acquired from triphasic enhanced CT. Additionally, we assessed the practicality and diagnostic performance of HU measurement on VUE images for assessing bone status, using QCT reports as the reference standard. Our results showed that there were no statistically significant

Table 4 ROC curve analysis of HU measurement for the diagnosis of osteopenia

Category	Threshold	Sensitivity, %	Specificity, %	AUC	95% CI
TUE	147.20	98.92	89.22	0.989	0.963–0.999
VUEa	64.05	84.95	98.04	0.971	0.936–0.990
VUEv	63.00	86.02	93.14	0.969	0.934–0.988
VUEd	65.20	89.25	90.20	0.971	0.937–0.990

ROC, receiver operating characteristic; HU, Hounsfield unit; TUE, true unenhanced; VUEa, VUE image from arterial phase; VUEv, VUE image from portal venous phase; VUEd, VUE image from delayed phase; AUC, area under the curve of receiver operating characteristic; CI, confidence interval.

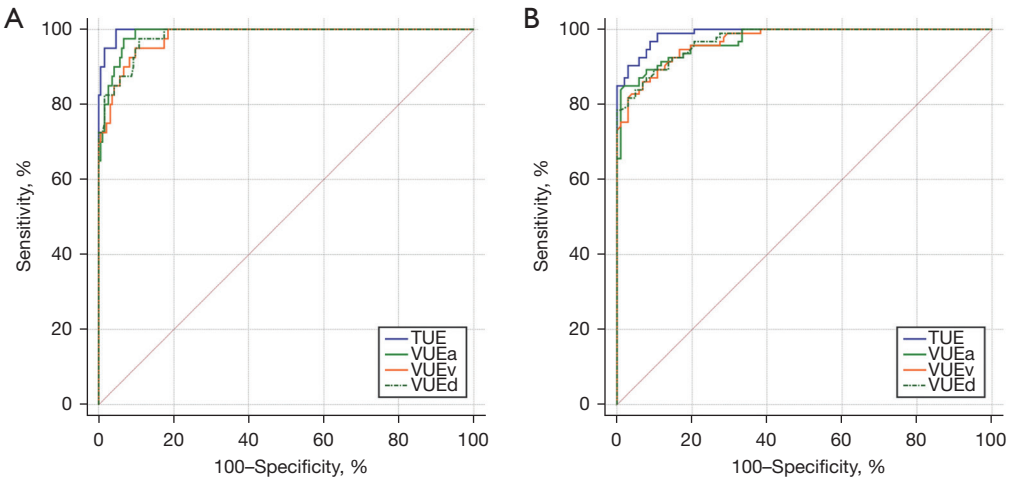

Figure 3 The ROC curves demonstrated that HU measurement had superior diagnostic performance in both TUE and VUE reconstructed triphasic enhanced CT. The DeLong test demonstrated a significant statistical difference between the TUE and triphasic VUE images for detecting osteoporosis. However, only on the VUE images reconstructed from venous phase and TUE was there a significant difference in distinguishing osteopenia. (A,B) The ROC curves for detecting osteoporosis and osteopenia. ROC, receiver operating characteristic; HU, Hounsfield unit; TUE, true unenhanced; VUE, virtual unenhanced; VUEa, VUE image from arterial phase; VUEv, VUE image from portal venous phase; VUEd, VUE image from delayed phase.

Table 5 The difference in the diagnosis of osteoporosis and osteopenia in TUE and triphasic VUE images

Category	Osteoporosis		Osteopenia		Z score	P value
	AUC	95% CI	AUC	95% CI		
TUE	0.997	0.978–1.000	0.989	0.963–0.999	1.469	0.1417
VUEa	0.988	0.964–0.998	0.971	0.936–0.990	1.598	0.1100
VUEv	0.979	0.952–0.993	0.969	0.934–0.988	0.832	0.4055
VUEd	0.982	0.956–0.995	0.971	0.937–0.990	0.917	0.3592

TUE, true unenhanced; VUE, virtual unenhanced; VUEa, VUE image from arterial phase; VUEv, VUE image from portal venous phase; VUEd, VUE image from delayed phase; AUC, area under the receiver operating characteristic curve; CI, confidence interval.

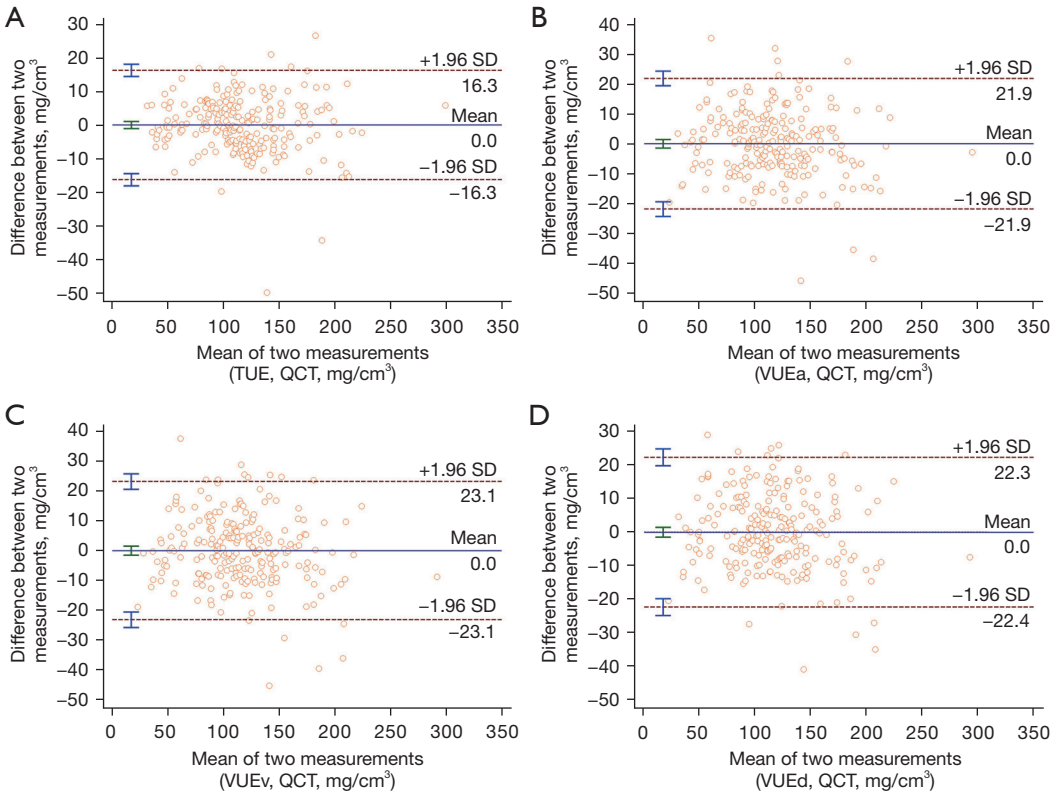

Figure 4 Bland-Altman plots showed that the BMD calculated by TUE and triphasic VUE linear equations were in good agreement with the reference BMD derived from QCT. The mean difference and limits of agreement are shown in with solid line and dotted line, respectively. SD, standard deviation; TUE, true unenhanced; QCT, quantitative computed tomography; VUE, virtual unenhanced; VUEa, VUE image from arterial phase; VUEv, VUE image from portal venous phase; VUEd, VUE image from delayed phase; BMD, bone mineral density.

differences in the CT attenuation values of the L1–L2 vertebrae between the VUE images. Although these values were significantly underestimated compared to those obtained from TUE images, strong linear correlations were found between HU measurements acquired from TUE and VUE images and the BMD values measured by QCT. Further, we demonstrated the usefulness of VUE images in BMD assessment, with the average CT attenuation values of the L1–L2 vertebrae on both TUE and VUE images demonstrating high diagnostic performance (AUC >0.95).

Based on the clinical profiles, individuals at high risk for osteoporosis (such as those with fractures, older adult individuals, and those with low bone mass) should receive continuous monitoring or specific intervention treatments (21). Neglecting strategic intervention measures may lead to a vicious cycle of recurrent fractures, potentially resulting in disability or premature death (22,23). CT images can provide valuable information regarding potential BMD, and using preexisting imaging data can aid in the efficient and cost-effective screening of osteoporosis. Several studies have already been published on this topic, including those involving cardiac CT (24), CT colonography (9), and abdominal CT acquired for other medical reasons (25).

HU measurement of the vertebrae is considered to be a straightforward and easily adaptable method for BMD assessment, exhibiting good repeatability both within and between evaluators (26). In this study, we observed excellent repeatability in HU measurements on both TUE images and triphasic VUE images (ICC >0.92). Moreover, a robust positive association was found between HU measurements from either TUE or VUE images and BMD, furnishing objective evidence for the application of HU measurement in opportunistic screening. With BMD measured with QCT as the reference standard, a threshold of 108.65 HU on TUE images was applied to differentiate osteoporosis, yielding a sensitivity of 100%, a specificity of 95.4%, and an AUC of 0.997. This finding is consistent with Pickhardt *et al.*'s study (25), involving a larger population of 1,867

adults, which found that a threshold of 110 HU in the L1 vertebra had a specificity exceeding 90% for the diagnosis of osteoporosis. However, Buckens *et al.* (27) used DXA as a reference standard and showed superior diagnostic performance at <99 HU for the L1 vertebra (AUC 0.74). This phenomenon may be attributed to multiple causes, such as differences in scanning equipment, benchmark standards, and the group being studied. Compared to DXA, QCT is less susceptible to factors of vascular wall calcification, degenerative changes, and vertebral compression fractures. Additionally, QCT offers superior precision and diagnostic validity. Hence, we opted for QCT as the reference method to assess BMD. The use of VUE images produced via material decomposition algorithms is expected to replace TUE images, as this may reduce radiation exposure, speed up scanning, and increase cost-effectiveness. Some studies have shown that CT attenuation values of abdominal tissues (liver, spleen, and kidney) in the VUE images reconstructed from the arterial phase are overestimated, while the VUE images from the portal phase are more accurate (16,28,29). We thus sought to determine which phase was most appropriate for reconstructing VUE images in dynamic enhanced CT for BMD assessment. Therefore, we conducted a careful assessment of vertebral HU measurement differences between the TUE and VUE images produced from the triphasic enhanced CT. Our findings showed that the CT attenuation values of the vertebrae were significantly lower in the 3-phase VUE images than those in the TUE images. Notably, no significant difference was found in the CT attenuation values of the vertebral body among the 3 types of VUE images. Therefore, our findings may be indicative of a more robust outcome. Similarly, Ding *et al.* (30) also observed a significant underestimation in the attenuation values of the L1 vertebral body when analyzing the reconstruction from VUE images in the portal phase in comparison to the corresponding TUE images (51.9±25.7 *vs.* 103.6±41.3 HU). The relative difference between the 2 values was observed to be approximately –52.6%±13.0%, which is consistent with our findings. VUE images are generated using multiple material decomposition algorithms, which facilitate the identification of iodine contrast agents in the enhanced CT images and virtually eliminate the corresponding influence of iodine on tissue CT attenuation. However, the effectiveness of iodine component removal may be influenced by a range of factors, including the choice of substance separation algorithm, scanning equipment, and contrast media protocol (18,31,32). Due to the similarly high attenuation characteristics of calcium and iodine, VUE images may exhibit suboptimal separation and oversubtraction of iodine levels, thereby leading to the elimination of voxels that contain calcium (33,34). VUE images have been reported to present inherent inaccuracies in the determination of calcification or stone volume and to exhibit limited sensitivity for smaller stones (35,36).

Although there might have been an underestimation of the attenuation value of the vertebral body on VUE images in our study, a strong positive correlation was still observed between the HU measurement of VUE images and the standard BMD measurement, which is consistent with the findings of Ding *et al.* (30) for virtual images reconstructed in the portal phase. These results indicated that the attenuation value of the vertebral body on VUE images may serve as a highly sensitive marker of variations in bone quality, presenting a valuable and potentially informative measure of BMD. Our findings highlight the clinical significance of VUE scans in assessing bone health. Moreover, the diagnostic efficacy analysis, with BMD as the reference standard, indicated that HU measurement had excellent diagnostic performance in both TUE and VUE images reconstructed from triphasic enhanced CT, accurately distinguishing osteoporosis from non-osteoporosis with an area under the ROC curve exceeding 0.97 and a sensitivity over 95%. The DeLong test revealed no statistically significant difference in the diagnostic efficacy of the 3-phase VUE images. Hence, to meet the various clinical demands, the choice of first-phase enhanced images for reconstruction may be arbitrary, increasing the applicability of the VUE images. In individuals with a high susceptibility to osteoporosis, using more highly sensitive thresholds cautiously may lead to positive clinical outcomes (12,37). The attenuation information of the vertebral body on VUE images can be an effective tool for quickly identifying those at a high risk of osteoporosis and successfully countering underdiagnosis, without the need for a specific QCT examination.

Furthermore, dual-energy spectral CT, using a single X-ray tube with fast switching between tube voltages of 80 and 140 kVp, facilitates the acquisition of various material densities (e.g., iodine, water, calcium) as additional diagnostic information. However, the technology does not allow for switching tube current or using automatic tube current modulation during the scanning process. Currently, it remains unclear whether altering the tube current would impact VUE image quality in clinical studies. Therefore, we employed a standard DECT enhanced scanning protocol

in our study. The DLP was 512.07±123.21 mGy·cm, which was within the range of values reported in the reference guidelines (460–1,200 mGy·cm) (38). In future studies, it may be possible to stratify patients based on their BMI in order to investigate the potential impact of radiation dose on the image quality of VUE.

There are several limitations to this study. First, we did not measure the attenuation value of the vertebral body in the triphasic enhanced images. It is worth noting that previous studies have reported on the amplitude or range of increase in the attenuation value of the vertebral body after the enhanced scan. Second, the sample size of our study was relatively small and limited to a single center. Further investigations with larger, multicenter populations are needed to establish more precise diagnostic thresholds. Reproducibility across different CT machines and scanning ranges is a potential limitation of our study. It is possible that different CT machines employ varying calibration methods, resulting in differences in HU values and potentially affecting the diagnostic accuracy.

In conclusion, despite the underestimation of the vertebral body attenuation values on VUE images compared to TUE images, our findings indicate that HU measurements on VUE images are effective for assessing BMD and detecting osteoporosis and osteopenia with good diagnostic performance.

Acknowledgments

We would like to thank Dr. Jianying Li for proofreading the manuscript and providing suggestions.
Funding: None.

Footnote

Conflicts of Interest: All authors have completed the ICMJE uniform disclosure form (available at https://qims.amegroups.com/article/view/10.21037/qims-23-748/coif). The authors have no conflicts of interest to declare.

Ethical Statement: The authors are accountable for all aspects of the work in ensuring that questions related to the accuracy or integrity of any part of the work are appropriately investigated and resolved. The study was conducted in accordance with the Declaration of Helsinki (as revised in 2013) and was approved by Ethics Committee of First Affiliated Hospital of Dalian Medical University (No. PJ-KS-KY-2022-43). All patients provided signed informed consent for use of their CT images.

References

1. Leslie WD, Morin SN. Osteoporosis epidemiology 2013: implications for diagnosis, risk assessment, and treatment. Curr Opin Rheumatol 2014;26:440-6.
2. Chen P, Li Z, Hu Y. Prevalence of osteoporosis in China: a meta-analysis and systematic review. BMC Public Health 2016;16:1039.
3. Lewiecki EM, Ortendahl JD, Vanderpuye-Orgle J, Grauer A, Arellano J, Lemay J, Harmon AL, Broder MS, Singer AJ. Healthcare Policy Changes in Osteoporosis Can Improve Outcomes and Reduce Costs in the United States. JBMR Plus 2019;3:e10192.
4. Burge R, Dawson-Hughes B, Solomon DH, Wong JB, King A, Tosteson A. Incidence and economic burden of osteoporosis-related fractures in the United States, 2005-2025. J Bone Miner Res 2007;22:465-75.
5. Bolotin HH. DXA in vivo BMD methodology: an erroneous and misleading research and clinical gauge of bone mineral status, bone fragility, and bone remodelling. Bone 2007;41:138-54.
6. Dimai HP. Use of dual-energy X-ray absorptiometry (DXA) for diagnosis and fracture risk assessment; WHO-criteria, T- and Z-score, and reference databases. Bone 2017;104:39-43.
7. Li Y, Jiang Y, Yu X, Ren B, Wang C, Chen S, Ma D, Su D, Liu H, Ren X, Yang X, Gao J, Wu Y. Deep-learning image reconstruction for image quality evaluation and accurate bone mineral density measurement on quantitative CT: A phantom-patient study. Front Endocrinol (Lausanne) 2022;13:884306.
8. Wu Y, Jiang Y, Han X, Wang M, Gao J. Application of low-tube current with iterative model reconstruction on Philips Brilliance iCT Elite FHD in the accuracy of spinal QCT using a European spine phantom. Quant Imaging Med Surg 2018;8:32-8.

9. Pickhardt PJ, Lee LJ, del Rio AM, Lauder T, Bruce RJ, Summers RM, Pooler BD, Binkley N. Simultaneous screening for osteoporosis at CT colonography: bone mineral density assessment using MDCT attenuation techniques compared with the DXA reference standard. J Bone Miner Res 2011;26:2194-203.
10. Budoff MJ, Malpeso JM, Zeb I, Gao YL, Li D, Choi TY, Dailing CA, Mao SS. Measurement of phantomless thoracic bone mineral density on coronary artery calcium CT scans acquired with various CT scanner models. Radiology 2013;267:830-6.
11. Link TM, Koppers BB, Licht T, Bauer J, Lu Y, Rummeny EJ. In vitro and in vivo spiral CT to determine bone mineral density: initial experience in patients at risk for osteoporosis. Radiology 2004;231:805-11.
12. Pickhardt PJ, Lauder T, Pooler BD, Muñoz Del Rio A, Rosas H, Bruce RJ, Binkley N. Effect of IV contrast on lumbar trabecular attenuation at routine abdominal CT: correlation with DXA and implications for opportunistic osteoporosis screening. Osteoporos Int 2016;27:147-52.
13. Dalla Via J, Daly RM, Owen PJ, Mundell NL, Rantalainen T, Fraser SF. Bone mineral density, structure, distribution and strength in men with prostate cancer treated with androgen deprivation therapy. Bone 2019;127:367-75.
14. Melton LJ 3rd, Lieber MM, Atkinson EJ, Achenbach SJ, Zincke H, Therneau TM, Khosla S. Fracture risk in men with prostate cancer: a population-based study. J Bone Miner Res 2011;26:1808-15.
15. Mergen V, Racine D, Jungblut L, Sartoretti T, Bickel S, Monnin P, Higashigaito K, Martini K, Alkadhi H, Euler A. Virtual Noncontrast Abdominal Imaging with Photon-counting Detector CT. Radiology 2022;305:107-15.
16. Ananthakrishnan L, Rajiah P, Ahn R, Rassouli N, Xi Y, Soesbe TC, Lewis MA, Lenkinski RE, Leyendecker JR, Abbara S. Spectral detector CT-derived virtual non-contrast images: comparison of attenuation values with unenhanced CT. Abdom Radiol (NY) 2017;42:702-9.
17. Sauter AP, Muenzel D, Dangelmaier J, Braren R, Pfeiffer F, Rummeny EJ, Noël PB, Fingerle AA. Dual-layer spectral computed tomography: Virtual non-contrast in comparison to true non-contrast images. Eur J Radiol 2018;104:108-14.
18. Choi MH, Lee YJ, Choi YJ, Pak S. Dual-energy CT of the liver: True noncontrast vs. virtual noncontrast images derived from multiple phases for the diagnosis of fatty liver. Eur J Radiol 2021;140:109741.
19. Engelke K, Lang T, Khosla S, Qin L, Zysset P, Leslie WD, Shepherd JA, Shousboe JT. Clinical Use of Quantitative Computed Tomography-Based Advanced Techniques in the Management of Osteoporosis in Adults: the 2015 ISCD Official Positions-Part III. J Clin Densitom 2015;18:393-407.
20. American College of Radiology (2018). ACR–SPR–SSR practice parameter for the performance of musculoskeletal quantitative computed tomography (QCT). Accessed 7 Nov 2018. Available online: https://www.acr.org/-/media/ACR/Files/Practice-Parameters/QCT.pdf?la=en
21. LeBoff MS, Greenspan SL, Insogna KL, Lewiecki EM, Saag KG, Singer AJ, Siris ES. The clinician's guide to prevention and treatment of osteoporosis. Osteoporos Int 2022;33:2049-102.
22. Cosman F, de Beur SJ, LeBoff MS, Lewiecki EM, Tanner B, Randall S, Lindsay R; . Clinician's Guide to Prevention and Treatment of Osteoporosis. Osteoporos Int 2014;25:2359-81.
23. Brown C. Osteoporosis: Staying strong. Nature 2017;550:S15-7.
24. Budoff MJ, Hamirani YS, Gao YL, Ismaeel H, Flores FR, Child J, Carson S, Nee JN, Mao S. Measurement of thoracic bone mineral density with quantitative CT. Radiology 2010;257:434-40.
25. Pickhardt PJ, Pooler BD, Lauder T, del Rio AM, Bruce RJ, Binkley N. Opportunistic screening for osteoporosis using abdominal computed tomography scans obtained for other indications. Ann Intern Med 2013;158:588-95.
26. Pompe E, de Jong PA, de Jong WU, Takx RA, Eikendal AL, Willemink MJ, Oudkerk M, Budde RP, Lammers JW, Mohamed Hoesein FA. Inter-observer and inter-examination variability of manual vertebral bone attenuation measurements on computed tomography. Eur Radiol 2016;26:3046-53.
27. Buckens CF, Dijkhuis G, de Keizer B, Verhaar HJ, de Jong PA. Opportunistic screening for osteoporosis on routine computed tomography? An external validation study. Eur Radiol 2015;25:2074-9.
28. Jamali S, Michoux N, Coche E, Dragean CA. Virtual unenhanced phase with spectral dual-energy CT: Is it an alternative to conventional true unenhanced phase for abdominal tissues? Diagn Interv Imaging 2019;100:503-11.
29. Zhang LJ, Peng J, Wu SY, Wang ZJ, Wu XS, Zhou CS, Ji XM, Lu GM. Liver virtual non-enhanced CT with dual-source, dual-energy CT: a preliminary study. Eur Radiol 2010;20:2257-64.
30. Ding Y, Richter A, Stiller W, Kauczor HU, Weber TF. Association between true non-contrast and virtual non-contrast vertebral bone CT attenuation values determined

using dual-layer spectral detector CT. Eur J Radiol 2019;121:108740.
31. Jing M, Sun J, Xi H, Liu Z, Zhang S, Deng L, Han T, Zhang B, Lin X, Zhou J. Abdominal virtual non-contrast images derived from energy spectrum CT to evaluate chemotherapy-related fatty liver disease. Quant Imaging Med Surg 2023;13:669-81.
32. Decker JA, Bette S, Scheurig-Muenkler C, Jehs B, Risch F, Woźnicki P, Braun FM, Haerting M, Wollny C, Kroencke TJ, Schwarz F. Virtual Non-Contrast Reconstructions of Photon-Counting Detector CT Angiography Datasets as Substitutes for True Non-Contrast Acquisitions in Patients after EVAR-Performance of a Novel Calcium-Preserving Reconstruction Algorithm. Diagnostics (Basel) 2022.
33. Borggrefe J, Neuhaus VF, Le Blanc M, Grosse Hokamp N, Maus V, Mpotsaris A, Lennartz S, Pinto Dos Santos D, Maintz D, Abdullayev N. Accuracy of iodine density thresholds for the separation of vertebral bone metastases from healthy-appearing trabecular bone in spectral detector computed tomography. Eur Radiol 2019;29:3253-61.
34. Abdullayev N, Große Hokamp N, Lennartz S, Holz JA, Romman Z, Pahn G, Neuhaus V, Maintz D, Krug B, Borggrefe J. Improvements of diagnostic accuracy and visualization of vertebral metastasis using multi-level virtual non-calcium reconstructions from dual-layer spectral detector computed tomography. Eur Radiol 2019;29:5941-9.
35. Lundin M, Lidén M, Magnuson A, Mohammed AA, Geijer H, Andersson T, Persson A. Virtual non-contrast dual-energy CT compared to single-energy CT of the urinary tract: a prospective study. Acta Radiol 2012;53:689-94.
36. Goo HW, Goo JM. Dual-Energy CT: New Horizon in Medical Imaging. Korean J Radiol 2017;18:555-69.
37. Woisetschläger M, Chisalita S, Vergara M, Spångeus A. Selection of risk assessment methods for osteoporosis screening in postmenopausal women with low-energy fractures: A comparison of fracture risk assessment tool, digital X-ray radiogrammetry, and dual-energy X-ray absorptiometry. SAGE Open Med 2022;10:20503121211073421.
38. Bos D, Yu S, Luong J, Chu P, Wang Y, Einstein AJ, et al. Diagnostic reference levels and median doses for common clinical indications of CT: findings from an international registry. Eur Radiol 2022;32:1971-82.

Cite this article as: Tong X, Fang X, Wang S, Fan Y, Wei W, Xiao Q, Chen A, Liu Y, Liu L. Virtual unenhanced images derived from dual-energy computed tomography for assessing bone mineral density and detecting osteoporosis. Quant Imaging Med Surg 2023;13(10):6571-6582. doi: 10.21037/qims-23-748

